GPS Solut
DOI 10.1007/s10291-015-0468-y

ORIGINAL ARTICLE

Integrity monitoring-based ratio test for GNSS integer ambiguity validation

Liang Li[1,2] · Zishen Li[1,3] · Hong Yuan[1] · Liang Wang[1] · Yanqing Hou[4]

Received: 15 October 2014 / Accepted: 2 June 2015

Abstract The combination of multiple global navigation satellite systems (GNSSs) is able to improve the accuracy and reliability, which is beneficial for navigation in safety–critical applications. Due to the relatively low accuracy of pseudorange observations, the single-epoch GNSS real-time kinematic (RTK) using phase observations can be utilized to achieve centimeter accuracy positioning instantaneously. Since the traditional ratio tests for ambiguity validation are not reliable in the presence of biases, it is therefore difficult for the single-epoch RTK to achieve high precision and high reliability, simultaneously. Instead of using an empirical constant detection threshold or a fixed failure/success rate requirement in the ratio tests for ambiguity validation, we propose an integrity monitoring-based ratio test (IM-RT). It uses the ambiguity protection level to control the false alarm and missed detection errors. The performance of the proposed method is tested by using simulated and real-world data. The simulation results show that the IM-RT can obtain an optimal balance between the false alarm and missed detection performance. The experiments from kinematic real-world data indicate that the IM-RT improves the positioning accuracy by over 10 cm and enhances the continuity by 11 %, when compared with the fixed detection threshold-based ratio test.

Keywords Ambiguity validation · Integrity monitoring · Ratio test · Real-time kinematic · GNSS

Introduction

Real-time kinematic (RTK) is a commonly used, high-precision positioning technology that has been shown to be efficient and reliable. However, its performance for safety-of-life (SoL) applications is affected by at least two issues. First, the positioning continuity dramatically deteriorates under challenging conditions caused by dynamics or poor receiving environments. This results in partial losses of tracked satellite signals and discontinuities in the ambiguities, i.e., cycle slip. Thus, cycle slips must be detected and repaired when using the traditional multi-epoch-based approach, and otherwise, the positioning is discontinuous. The single-epoch/instantaneous positioning can avoid this limitation because it is immune to cycle slip. Therefore, it is preferable for the real-time operations. Furthermore, the false rejection of a correctly fixed ambiguity (i.e., a Type I error constrained by the probability of false alarm) can also lead to discontinuities of positioning. Additionally, the failure to reject an incorrectly fixed ambiguity (i.e., a Type II error controlled by the probability of missed detection) yields hazardously misleading information. Thus, when using RTK for safety–critical navigation, we must apply rigorous ambiguity validation processes that simultaneously control Type I and Type II errors. Most existing

✉ Liang Li
liliang@hrbeu.edu.cn

✉ Zishen Li
lizishen@aoe.ac.cn

Yanqing Hou
h.yanqing@tudelft.nl

[1] Academy of Opto-electronics, Chinese Academy of Sciences, Beijing 100094, China

[2] College of Automation, Harbin Engineering University, Harbin 150001, China

[3] State Key Laboratory of Geodesy and Earth's Dynamics, Institute of Geodesy and Geophysics, Chinese Academy of Sciences, Wuhan, China

[4] Delft University of Technology, Delft, The Netherlands

Published online: 17 June 2015

ambiguity validation methods can be categorized into the following three groups.

1. The first group is implemented in the ambiguity domain and includes the ratio test (Leick et al. 2015; Teunissen and Verhagen 2009), the difference test (Tiberius and Jonge 1995), the *F*-ratio test (Euler and Schaffrin 1991), the *W*-ratio test (Wang et al. 1998), and the projector test (Han 1997). These methods use the test statistics constructed from the best and second-best ambiguity candidates.
2. The second group of methods aims at verifying that the success rate of the ambiguity resolution (AR) is sufficiently high or the failure rate is low enough. The estimates of either the upper or lower bound of the success rate are commonly used by integer estimators (Li and Wang 2014), where the integer least square estimator has the highest success rate. Therefore, this approach is a quantitative evaluation in the probability domain.
3. The third group constructs the horizontal/vertical protection level to evaluate the performance of AR, using advanced/relative receiver autonomous integrity monitoring in the position domain (Khanafseh and Pervan 2010).

There are potentially multiple faults in the range domain, which undermine the integrity performance of position domain-based methods. Therefore, the ambiguity validation methods in the probability and ambiguity domains are often sequentially applied to test the reliability of AR with a predefined confidence level. Specifically, the probability domain-based methods typically use a high success rate to assess the confidence level. If the success rate requirement is satisfied, the ambiguity domain-based methods verify whether or not the best ambiguity candidate is sufficiently more likely to be correct than the second best, according to an empirical threshold value. However, these methods are carried out under the bias-free hypothesis. This is acceptable if observation biases can be prevented. Potential biases such as ionospheric and tropospheric errors are always present in the ambiguity estimation model under challenging navigation environments. The ambiguity can be fixed incorrectly without using an efficient test. The biased ambiguity can propagate in the position domain and result in unacceptable positioning error. Consequently, the power of the sequential validation method can be undermined because of arbitrary missed detection rates that result from a biased AR. Additionally, previously estimated uncalibrated phase delays (UPDs) are typically biased, so the UPD-corrected ambiguities at the precise point positioning (PPP) stations are biased (Ge et al. 2008). Thus, the PPP efficiency can be undermined if an efficient ambiguity validation test is not used. Li et al. (2014) showed that a precise characterization of the biases yields a higher AR success rate. However, the evaluation of bias-affected AR depends on a priori knowledge of the biases, which may be difficult to acquire in real-world applications. The false alarm (Type I) and missed detection (Type II) errors (DeGroot and Schervish 2011) are two key parameters that must be controlled by the integrity monitoring approach. This naturally leads us to consider applying the integrity monitoring approach for ambiguity validation. Therefore, we have investigated a new integrity monitoring-based ratio test for ambiguity validation, which simultaneously satisfies the predefined false alarm rate under the fault-free hypothesis and the missed detection rate under the fault hypothesis.

The positioning accuracy and reliability can be improved by solving full ambiguity vectors. However, because of potentially severe observation noise and/or biases, it is difficult to fix a full ambiguity vector with a sufficiently low probability of false fixing (Verhagen et al. 2010). If the ambiguity is biased because of low-quality carrier phase measurements, the accuracy of fixed position solution will be jeopardized inevitably. Furthermore, the rapid development of emerging GNSS systems such as BeiDou navigation satellite system (BDS) and Galileo means that the real-time performance suffers from heavy computation burden because there has been a dramatic increase in available satellites. To fix these problems, a subset of decorrelated float ambiguities can be preferentially fixed so that the high-quality carrier phase measurements can be ultimately used without sacrificing the real-time performance. Therefore, the partial ambiguity resolution (PAR) method is applied for safety–critical applications. Because we can select the subset of ambiguities based on many criteria, e.g., elevation, signal-to-noise ratio, and minimum success rate requirement (MSSR) (Parkins 2011), there will be a negative impact on the real-time performance if we consider all the factors. In this research, the PAR method is carried out based on the MSSR criterion. Details of the PAR implementation can be found in Teunissen et al. (1999).

We first discuss the limitations of success rate and traditional ratio tests when validating ambiguity reliability, followed by a description of the integrity monitoring-based ratio test. We present and analyze simulation and real-world experimental results and summarize the research findings.

Limitations of the success rate criterion and the traditional ratio test

The success rate and traditional ratio test are commonly used to test the reliability of AR. Nevertheless, these methods have limitations when used to simultaneously

control Type I and Type II errors, as will be discussed next. So that we can distinguish it from the observation bias, the bias in the following analysis is assumed to be in the ambiguity domain if it is expressed without a further description.

The baseline concept of the success rate

The success rate is defined as the probability that the float ambiguity solution is fixed to the correct integer ambiguity vector. Provided that the float ambiguity vector is Gaussian distributed, the success rate under the bias-free hypothesis can be computed using (Li et al. 2014)

$$P_{\mathrm{s}} = P\left(\breve{\mathbf{z}} = \mathbf{z}\right) = P(\hat{\mathbf{z}} \in S_{\mathbf{z}}) = \int_{S_{\mathbf{z}}} f_{\hat{\mathbf{z}}}(\mathbf{x};\mathbf{z})\mathrm{d}\mathbf{x} \tag{1}$$

where $\mathbf{z}$ is the correct integer ambiguity vector and $S_{\mathbf{z}}$ is the pull-in region where all real-valued float ambiguity vectors $\hat{\mathbf{z}}$ will be mapped to integer vector $\breve{\mathbf{z}}$ (Teunissen et al. 1999). Under the Gaussian distribution assumption, the probability density function (PDF) is

$$f_{\hat{\mathbf{z}}}(\mathbf{x};\mathbf{z}) = \frac{1}{\sqrt{(2\pi)^{n_p}|\mathbf{Q}_{\hat{\mathbf{z}}}|}} \exp\left\{-\frac{1}{2}\|\mathbf{x}-\mathbf{z}\|^2_{\mathbf{Q}_{\hat{\mathbf{z}}}^{-1}}\right\} \tag{2}$$

where $\|\cdot\|^2_{\mathbf{Q}} = (\cdot)^{\mathrm{T}}\mathbf{Q}^{-1}(\cdot)^{\mathrm{T}}$, $\mathbf{Q}_{\hat{\mathbf{z}}} = \mathbf{Z}^{\mathrm{T}}\mathbf{Q}_{\hat{\mathbf{a}}}\mathbf{Z}$, n_p is the number of fixed ambiguities elements, $\mathbf{Q}_{\hat{\mathbf{a}}}$ is the variance–covariance matrix of the float ambiguity solution $\hat{\mathbf{a}}$, and $\mathbf{Z}$ is the Z-transform matrix (Teunissen and Kleusberg 1998). We can derive the success rate of PAR under the bias-free hypothesis by combining (1) and (2). When considering the PAR under the bias-affected hypothesis, the biased float ambiguity solution follows the Gaussian distribution $\mathrm{N}\left(\mathbf{z}+\Delta\mathbf{z}, \mathbf{Q}^b_{\hat{\mathbf{z}}}\right)$, and the success rate can be calculated using (Li et al. 2014)

$$P_{s,b} = P\left(\breve{\mathbf{z}}^b = \mathbf{z}\right) = P\left(\hat{\mathbf{z}}^b \in S_{\mathbf{z}}\right) = \int_{S_{\mathbf{z}}} f_{\hat{\mathbf{z}}^b}(\mathbf{x};\mathbf{z})\mathrm{d}\mathbf{x} \tag{3}$$

$$f_{\hat{\mathbf{z}}^b}(\mathbf{x};\mathbf{z}) = \frac{1}{\sqrt{(2\pi)^{n_p}|\mathbf{Q}^b_{\hat{\mathbf{z}}}|}} \exp\left\{-\frac{1}{2}\|\mathbf{x}-\mathbf{z}-\Delta\mathbf{z}\|^2_{(\mathbf{Q}^b_{\hat{\mathbf{z}}})^{-1}}\right\} \tag{4}$$

$$\Delta\mathbf{z} = \mathbf{Z}^{\mathrm{T}}\Delta\mathbf{a} \tag{5}$$

where $\Delta\mathbf{a}$ is the ambiguity bias caused by the observation bias, and superscript b indicates the bias-affected case. To precisely evaluate the reliability of a bias-affected AR, we must know the bias model. However, this is not possible in real applications and undermines the efficiency of the success rate-based evaluation method. A simple simulation is conducted to reveal the limitation of success rate in dealing with an unknown bias (i.e., a biased observation model), when the success rate is based on the bias-free hypothesis.

Figure 1 shows the a priori computed success rate from (1) and the true success rate, for a biased ambiguity solution in four dimensions, $\hat{\mathbf{a}}_{\mathrm{b}} \sim \mathrm{N}(\boldsymbol{\mu}_{\hat{\mathbf{a}}}, \mathbf{Q}_{\hat{\mathbf{a}}})$, with varying the biases μ_a and precisions σ_a,

$$\boldsymbol{\mu}_{\hat{\mathbf{a}}} = \mu_a \cdot \mathbf{1}_{4\times 1}, \quad \mathbf{Q}_{\hat{\mathbf{a}}} = 0.5 \cdot \sigma_a^2 \cdot (\mathbf{I}_4 + \mathbf{1}_{4\times 4}),$$

where $\mathbf{I}$ is the identity matrix and $\mathbf{1}$ is a matrix of ones. This simulation compares the performance of full ambiguity resolution (FAR) and PAR. The MSSR for PAR is set to 99 %.

Figure 1 shows that the computed success rate only depends on the precision of the ambiguity float solution

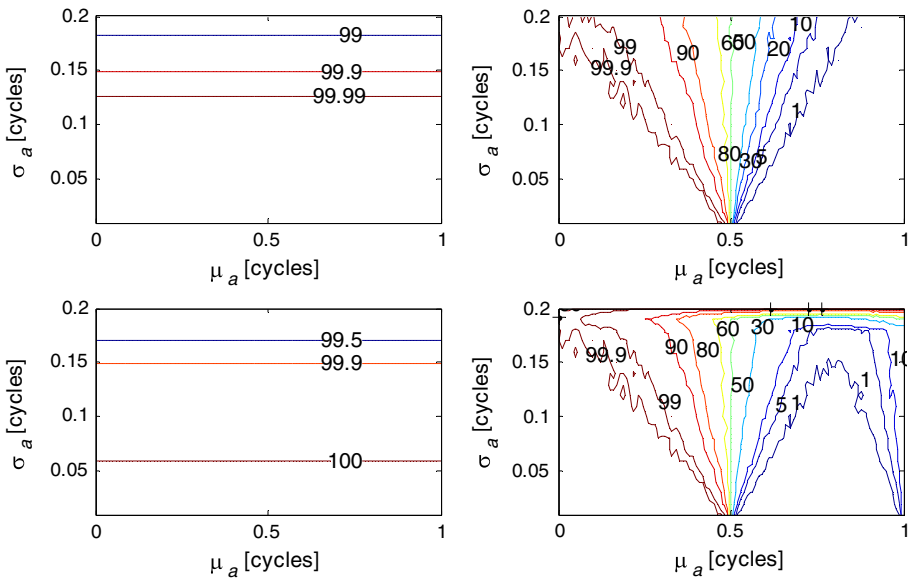

Fig. 1 Computed success rates (CSR) and true success rates (TSR) with FAR and PAR. *Top left* CSR with FAR, *top right* TSR with FAR, *bottom left* CSR with PAR, *bottom right* TSR with PAR

under the bias-free hypothesis. Since the true ambiguity solution is known, we can obtain the true success rate using posteriori statistics. However, the true success rate not only interacts with the precision, but also is influenced by the bias for both the FAR and PAR. The figure demonstrates that the difference between the true and computed success rates increases with μ_a, which indicates that there are many missed detections and false alarms. Additionally, it can be found that the PAR is more robust than the FAR in the presence of larger biases and lower precision (e.g., $\mu_a > 0.8$ cycle and $\sigma_a > 0.15$ cycle), which also implies the necessity of applying PAR in safety–critical applications.

The above analysis shows that the success rate calculated using (1) in the bias-affected case is not sufficiently accurate for evaluating the reliability of AR, particularly when there are larger biases. There are many alternative methods for checking the reliability of AR, e.g., ratio test, difference test, *W*-ratio test, and projection test, of which the ratio test is the most commonly used.

The traditional ratio test

The test statistic t for the traditional ratio test is

$$t = \frac{\Omega_o}{\Omega_s} \leq \mu \tag{6}$$

where

$$\Omega_o = \left\| \hat{\mathbf{z}} - \breve{\mathbf{z}}_o \right\|_{\mathbf{Q}_{\hat{\mathbf{z}}}^{-1}}, \quad \Omega_s = \left\| \hat{\mathbf{z}} - \breve{\mathbf{z}}_s \right\|_{\mathbf{Q}_{\hat{\mathbf{z}}}^{-1}} \tag{7}$$

and the subscripts o and s represent the best and second best. If Ω_s is at least $1/\mu$ times larger than Ω_o, the best ambiguity candidate is accepted. Otherwise, neither the best nor the second-best ambiguity candidate can be accepted as the ambiguity-fixed solution. It is clear that the threshold μ determines the performance of the ratio test associated with (6). The threshold μ is typically recommended as either an empirical fixed value used by the traditional ratio test (FT-RT) or a variable value used by the fixed failure rate ratio test (FF-RT). However, neither of these ratio tests can sufficiently verify the reliability of AR. The FT-RT can be either over-conservative or over-optimistic, which means that a correctly fixed ambiguity solution fails the test or an incorrectly fixed ambiguity solution passes. Although the FF-RT aims to constrain Type II error, Type I error cannot be controlled because the detection threshold can be arbitrarily strict to reduce the failure rate.

The integrity monitoring approach is developed to control the false alarm and missed detection errors simultaneously. This feature leads us to consider combining the integrity monitoring approach with the ratio test. The integrity monitoring approach for satellite navigation is conventionally carried out in either the position domain or range domain to verify the reliability of the position solution. In order to test the reliability of AR, a new integrity monitoring approach needs to be developed in the ambiguity domain.

Integrity monitoring-based ratio test (IM-RT)

The integrity monitoring approach considers the statistical distribution of the constructed test statistic under the respective bias-free and bias-affected hypotheses. In the ambiguity domain, the biases come from the incorrectly fixed ambiguity solutions that are caused by the inaccurate observation model characterization. The failure modes can be a collection of single or multiple incorrectly fixed ambiguity elements. A statistical test of the correctness of the best ambiguity candidate $\breve{\mathbf{z}}_o$ can be based on the following null hypothesis

$$\mathrm{H}_0 : \breve{\mathbf{z}}_o = \mathbf{z} \tag{8}$$

and the alternative hypothesis

$$\mathrm{H}_1 : \breve{\mathbf{z}}_o \neq \mathbf{z} \tag{9}$$

Under the bias-free hypothesis, Ω_o and Ω_s follow the Chi-square distribution, and so the ratio value t in (6) follows the Fisher distribution. Teunissen and Kleusberg (1998) noted that the Fisher distribution cannot be guaranteed, because of the correlation between Ω_o and Ω_s. The over-bounding approach can be applied to compensate for the non-perfect Fisher distribution, but this generates more integrity loss than expected (Lee et al. 2009). However, the integrity loss can be manipulated by choosing an appropriate inflation factor. Another important point is that the best ambiguity candidate is assumed to be correctly fixed under the bias-free hypothesis. Therefore, the second-best ambiguity candidate is fixed with bias. Correspondingly, Ω_o/n_p follows the central Chi-square distribution $\chi^2(0, n_p)$, and Ω_s/n_p follows the non-central Chi-square distribution $\chi^2(\delta_s, n_p)$. Here, the non-centrality parameter δ_s follows

$$\delta_s = \left(\breve{\mathbf{z}}_o - \breve{\mathbf{z}}_s\right)^{\mathrm{T}} \mathbf{Q}_{\hat{\mathbf{z}}}^{-1} \left(\breve{\mathbf{z}}_o - \breve{\mathbf{z}}_s\right) \tag{10}$$

where $\breve{\mathbf{z}}_s$ is the second-best ambiguity candidate. The ratio value under the bias-free hypothesis follows

$$t|H_0 \sim \mathrm{F}_t\left(n_p, n_p; 0, \delta_s\right) \tag{11}$$

where $F(\mathrm{dof}_1,\mathrm{dof}_2;\mathrm{delta}_1,\mathrm{delta}_2)$ is the PDF of the Fisher distribution. Here, dof_1 is the degree of freedom and delta_1 denotes the corresponding positive non-centrality parameters, and dof_2 is the degree of freedom in the denominator and delta_2 denotes the corresponding positive non-

centrality parameters. Note that $t < 1$ is always satisfied by the output of the LAMBDA algorithm, which means that the distribution of t is *truncated*. Therefore, the detection threshold T can be obtained from the predefined probability of false alarm P_{fa}. That is,

$$1 - P_{\text{fa}} = P(t < T|H_0) = \int_0^{\text{T}} \text{TrF}_x(n_p, n_p; 0, \delta_s)\text{d}x \tag{12}$$

$$\text{TrF}_x = \frac{F_x}{\int_0^1 F_x \text{d}x} \tag{13}$$

where TrF is the PDF of the truncated Fisher distribution. The detection result produced by comparing the ratio value t and the detection threshold T reflects the consistency between the data and bias-free hypothesis. Furthermore, the PDF of the non-central Fisher distribution implies that the detection threshold becomes looser with more sequentially fixed ambiguities. Thus, the PAR algorithm should fix as many ambiguities as possible because a looser detection threshold yields less false alarm rate. Although a looser detection threshold results in a smaller false alarm rate, the Type II errors will increase. The integrity monitoring approach controls Type II errors under the bias-affected hypothesis by satisfying the predefined probability of missed detection.

Under the bias-affected hypothesis, there are two failure modes:

1. In an extreme case, the best ambiguity candidate is biased, whereas the second-best ambiguity candidate is correct, i.e., $\Omega_o/n_p \sim \chi^2(n_p,\ \delta_o)$, $\Omega_s/n_p \sim \chi^2(n_p,\ 0)$, which yields

   $$t|H_{1,I} \sim \text{TrF}(n_p, n_p; \delta_o, 0) \tag{14}$$

   in which the non-centrality parameter δ_o follows from

   $$\delta_o = \left(\breve{\mathbf{z}}_s - \breve{\mathbf{z}}_o\right)^{\text{T}} \mathbf{Q}_{\hat{\mathbf{z}}}^{-1} \left(\breve{\mathbf{z}}_s - \breve{\mathbf{z}}_o\right) \tag{15}$$

2. In a general case, the best and second-best ambiguity candidates are both incorrect, so

   $$t|H_{1,II} \sim \text{TrF}(n_p, n_p; \delta'_o, \delta'_s) \tag{16}$$

   where δ'_o and δ'_s are the non-centrality parameters for Ω_o and Ω_s, respectively. Assuming that cases (1) and (2) are independent of each other, the probability of missed detection P_{md} can be computed using the detection threshold from (12),

   $$\begin{aligned} P_{\text{md}} &= P(t < T|H_1) = P_{\text{md},I} + P_{\text{md},II} \\ &= \int_0^{\text{T}} \text{TrF}_x(n_p, n_p; \delta_o, 0)\text{d}x \cdot \eta \\ &\quad + \int_0^{\text{T}} \text{TrF}_x(n_p, n_p; \delta'_o, \delta'_s)\text{d}x \cdot (1 - \eta), \end{aligned} \tag{17}$$

   where η is the prior probability of case (1) and should be chosen carefully because it affects the constraint of P_{md}. Note that the effect of a non-optimal η can be partially compensated by conservatively constructing the ambiguity protection level (APL).

The non-centrality parameter determines the biased ambiguity that can be detected, so we must solve for two unknown parameters, i.e., δ'_o and δ'_s with P_{md} in (17). Thus, another constraint on the non-centrality parameters has to be imposed. One solution is to set up two probabilities of missed detection to obtain δ'_o and δ'_s, as recommended by Feng et al. (2012). This method requires an a priori allocation of the total probability of missed detection for the best and second-best ambiguity candidates, which is another problem that must be solved. To avoid this, the constraint for δ'_o and δ'_s is determined by using the concept of worst-case protection, which is commonly used in the integrity monitoring approach (Hwang and Brown 2006).

In the next step, we construct an ambiguity protection level that is comparable to the protection level in the position domain-based integrity monitoring approach. The reliability of the AR can be split into two parts: the probability of the correct ambiguity solution passing the test and the probability of detecting the incorrectly fixed ambiguity. Thus, the reliability level of the AR can be computed using (DeGroot and Schervish 2011)

$$\begin{aligned} &\left(1 - \int_{t \in S_1} f(t|H_0)\text{d}t\right) P(H_0) + \left(1 - \int_{t \in S_0} f(t|H_1)\text{d}t\right) P(H_1) \\ &\quad = 1 - P(H_1) - \int_{t \in S_0} [P(H_0) f(t|H_0) - P(H_1) f(t|H_1)]\text{d}t \end{aligned} \tag{18}$$

where S_0 and S_1 are the acceptance and rejection regions for the test statistic. $P(H_0)$ and $P(H_1)$ are the priori probabilities of the null and alternative hypotheses. According to the maximum likelihood ratio, another test statistic APL for the ambiguity validation under the bias-affected hypothesis is

$$\begin{aligned} \text{APL} &= \frac{f(t|H_1)}{f(t|H_0)} \\ &= \frac{\eta \text{TrF}_t(n_p, n_p; \delta_o, 0) + (1 - \eta)\text{TrF}_t(n_p, n_p; \delta'_o, \delta'_s)}{\text{TrF}_t(n_p, n_p; 0, \delta_s)} \end{aligned} \tag{19}$$

As to the detection threshold for APL, the ambiguity alarm limit (AAL) can be set to $P(H_0)/P(H_1)$, where $P(H_0)$ is the computed success rate that indicates the strength of the observation model. There are two unknown non-centrality parameters, δ'_o and δ'_s, which determine the APL.

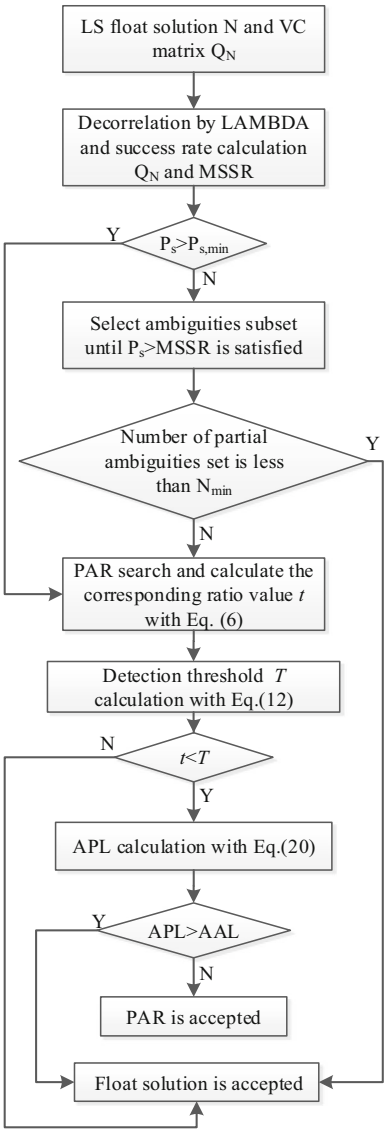

Fig. 2 Flowchart of IM-RT for PAR

According to the worst-case protection concept, we should select the non-centrality parameters that achieve the maximum APL, i.e.,

$$\mathrm{APL} = \frac{\eta \mathrm{TrF}_t\left(n_p, n_p; \delta_o, 0\right)}{\mathrm{TrF}_t\left(n_p, n_p; 0, \delta_s\right)} + \arg\max_{\delta_o', \delta_s'} \frac{(1-\eta)\mathrm{TrF}_t\left(n_p, n_p; \delta_o', \delta_s'\right)}{\mathrm{TrF}_t\left(n_p, n_p; 0, \delta_s\right)} \tag{20}$$

The first term in the right-hand side of (20) can be calculated using (15) and (10). The second term in the right-hand side of (20) satisfies $\delta_o' = \alpha\delta_s'$ or $\delta_s' = \alpha\delta_o'$, where $\alpha \in (0,1)$. Using the constraint in (17), δ_o' and δ_s' can be determined by iteratively searching for α.

The flowchart of the proposed IM-RT for PAR is shown in Fig. 2, in which $N_{\min}$ is the required minimum number of ambiguities that must be fixed. Unlike the success rate and ratio test concepts, the IM-RT provides double level of protection. That is, the first detection process compares the ratio value in (6) and the detection threshold in (12) to control Type I errors. Based on the test result of the first detection process, the second verification process compares the APL constructed in (20) and the AAL to constrain Type II errors. Therefore, the IM-RT is anticipated to obtain better ambiguity validation performance.

Experimental discussion

In order to reliably evaluate the proposed algorithm, the datasets must reflect a typical navigation environment. The Monte Carlo simulation approach was first carried out to create the respective bias-free and bias-affected cases. Then, the real-world experiment was conducted to make a comparison between the proposed IM-RT and the popular ambiguity validation methods.

Monte Carlo simulation results and analysis

We study the ambiguity validation performance of different methods with and without ionospheric correction errors. The zero-baseline 24-h GPS and BDS raw data are downloaded from saegnss2.curtin.edu.au/ldc. These data include the dual-frequency code and phase and have a sampling period of 30 s. The dual-frequency GPS and BDS observations are assumed to be independent. For all the tested ambiguity validation methods, the double-differenced ambiguities are processed with respect to each individual system. The cutoff elevation angel is set to 10°. The elevation-dependent weighting is applied, and the observation standard deviation (STD) at elevation θ is $\sigma_\varphi = \sigma_o(1 + 1/\sin\theta)$ with σ_o being the STD in zenith, which takes 3 mm and 30 cm for dual-frequency carrier phase and code, respectively.

The ionospheric error vector $\boldsymbol{\xi}$ is a function of the zenith ionospheric bias ξ_z, such that

$$\boldsymbol{\xi} = \mathbf{T}\mathbf{M}\xi_z \tag{21}$$

where $\mathbf{T}$ is the transform matrix converting the undifferenced ionospheric error to double-differenced errors. The mapping matrix $\mathbf{M}$ is the obliquity factor for projecting zenith ionospheric error ξ_z to the undifferenced slant ionospheric error as a function of ith elevation angle, i.e., $\mathbf{M}_i = \left[1 - \cos^2\theta_i/(1 + h/R)^2\right]^{-1/2}$ (Leick et al. 2015; Li et al. 2012), where R is the mean radius of the earth and h is the average height of the ionosphere layer. Inaccurate characterizations of ionospheric errors can affect the reliability of the ambiguity validation, so the zenith

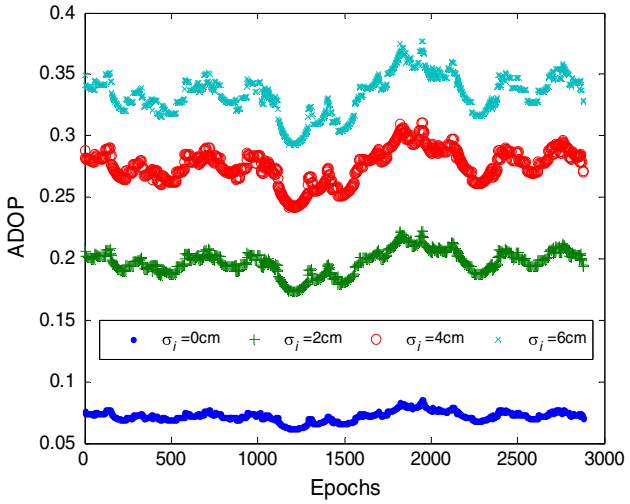

Fig. 3 ADOPs of four different ionosphere simulation cases

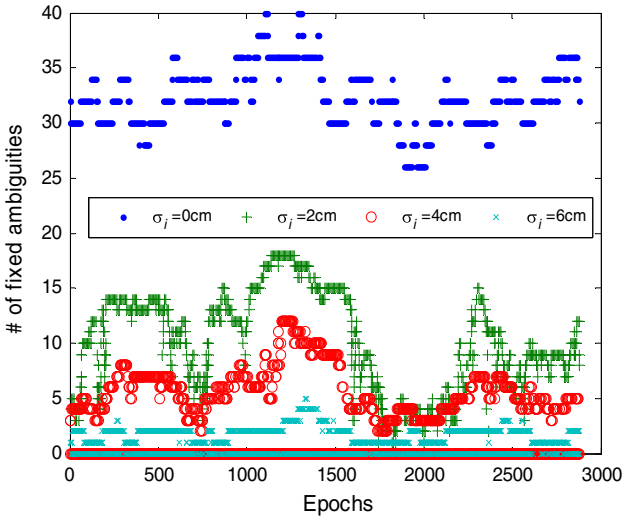

Fig. 4 Number of fixed ambiguities for four different ionosphere simulation cases

ionospheric errors are mapped to the undifferenced raw observations with STDs of 0, 2, 4, and 6, respectively. Ambiguity validation can be tested in the presence of inaccurate observations because the simulated ionospheric correction errors are not accounted for.

The FF-RT proposed by Verhagen and Teunissen (2013) performs well by using a variable detection threshold, so we compared it with the proposed IM-RT. The failure rate requirement for the FF-RT is set to 10^{-3}. The probabilities of false alarm and missed detection are set to 10^{-2} and 5×10^{-2}, respectively. The value of η is approximately derived from the posterior statistical results of the extreme case, i.e., case (1), and is set to 0.01. The ranges of δ_o' and δ_s' are derived from (5), and the search step length for α is 0.01 to reduce the computational burden. Verhagen et al. (2010) stated that MSSR is only over 99 % if the ambiguity dilution of precision (ADOP) is less than 0.15 cycles. This implies that the MSSR should be adjusted according to the ADOP value. If the success rate is constant without considering ADOP, there may be a considerably low number of fixed ambiguities and the positioning accuracy may be close to the float solution. Thus, in this simulation, the predefined MSSR is adjusted based on the ADOP, i.e., MSSR = 99 % if ADOP < 0.15 cycles, and MSSR = 90 % if ADOP ≥ 0.15 cycles.

The ADOP values for four different ionosphere simulations are shown in Fig. 3. The ADOP increased with the ionospheric errors, which implies that the observation model became weaker. The number of fixed ambiguities for the four simulation cases is shown in Fig. 4. The 90th percentile of the fixed ambiguities n_{par} is listed in Table 1. A larger ADOP value will result in a lower success rate; therefore, the number of fixed ambiguities decreases with an increase in ADOP. In the extreme case, none of the ambiguities can be fixed by the PAR process because it is difficult to satisfy the MSSR. Thus, the MSSR has to be adjusted according to ADOP.

Table 1 Statistical result of AR success rates, false alarm, missed detection under different simulation scenarios

	P_{CF}	P_{FA}	P_{MD}	n_{par} (90 %)	P_{scon}
$\sigma_\iota = 0$ cm, $P_s = 99$ %					
FT-RT(1.5)	100	0	0	30	100
FT-RT(2)	100	0	0	30	100
FT-RT(3)	100	0	0	30	100
FF-RT	100	0	0	30	100
IM-RT	100	0	0	30	100
$\sigma_\iota = 2$ cm, $P_s = 99$ %					
FT-RT(1.5)	98.82	0.31	0	4	100
FT-RT(2)	97.74	1.39	0	3	100
FT-RT(3)	88.89	10.24	0	0	100
FF-RT	98.68	0.45	0	4	100
IM-RT	99.13	0	0.03	4	99.96
$\sigma_\iota = 4$ cm, $P_s =$ 90 %					
FT-RT(1.5)	88.19	7.60	0.94	0	98.94
FT-RT(2)	79.62	16.18	0.45	0	99.43
FT-RT(3)	62.78	33.02	0.17	0	99.72
FF-RT	36.91	58.89	0.00	0	100
IM-RT	95.38	0.62	0.83	3	99.10
$\sigma_\iota = 6$ cm, $P_s = 90$ %					
FT-RT(1.5)	90.59	3.65	3.16	1	96.51
FT-RT(2)	87.08	7.15	2.12	0	97.57
FT-RT(3)	79.79	14.44	1.01	0	98.74
FF-RT	55.59	38.65	0.21	0	99.63
IM-RT	90.73	3.51	0.24	1	99.70

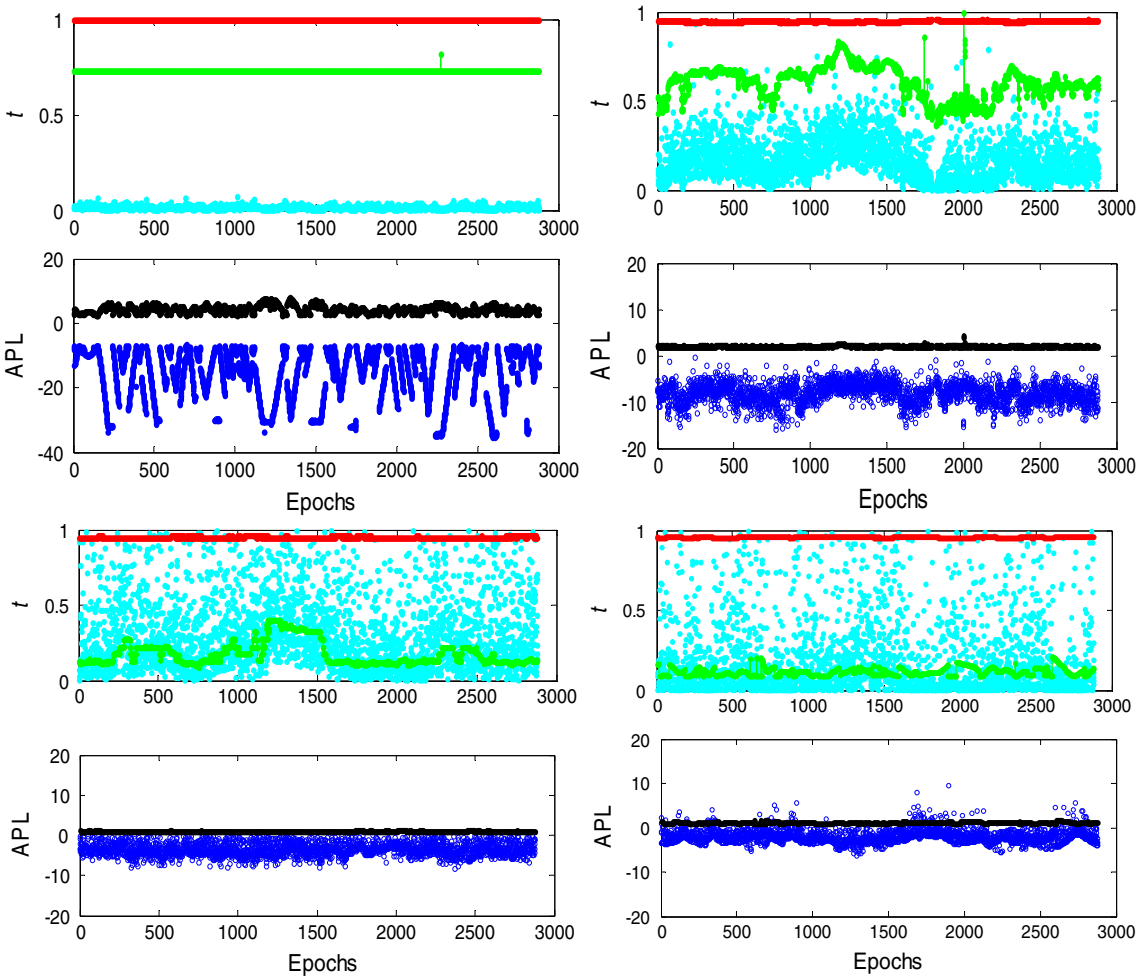

Fig. 5 Test process for four different ionosphere simulation cases. *Top left* $\sigma_\iota = 0$ cm, *top right* $\sigma_\iota = 2$ cm, *bottom left* $\sigma_\iota = 4$ cm, *bottom right* $\sigma_\iota = 6$ cm. The *cyan*, *green*, *red*, *blue,* and *black markers* represent the ratio value, the detection threshold of FF-RT, the detection threshold of IM-RT, the APL, and AAL, respectively

Fig. 6 Reference trajectory of the rover receiver

Figure 5 shows the test results of FF-RT and IM-RT under different ionosphere simulations. As the ionospheric correction error becomes more uncertain, the ratios become larger. To deal with the weaknesses of the observation model, the FF-RT applies a stricter detection threshold to avoid missed detections. However, this may also create

more false alarms. In contrast, the IM-RT uses a relatively loose detection threshold for larger ionospheric biases to prevent a large false alarm rate. Rather than using a single detection threshold, the IM-RT applies another test that compares the APL and AAL to detect the missed detections. In this way, the proposed IM-RT simultaneously controls Type I and Type II errors. It can be seen from the figure that the AAL decreases as the ionospheric error increases. This is because the AR success rate decreases when the uncertainty of the unaccounted ionospheric error increases, and the AAL accordingly decreases to reduce the number of missed detections.

To demonstrate the effectiveness of the proposed IM-RT, we compared the ambiguity validation performance of different ratio tests: the widely used FT-RT with fixed thresholds ($1/\mu$) of 1.5, 2, and 3, the FF-RT, and the proposed IM-RT. The ambiguity validation results are compared by using the correctly fixed rate P_{CF}, the true false alarm rate P_{FA}, and the true missed detection rate P_{MD}. Other statistical results for the ambiguity validation, such as the number of fixed ambiguities n_{par} and the conditional success rate P_{scon}, are also given in Table 1.

Table 1 shows that the cases of missed detections for the FT-RTs can be reduced by using a stricter detection threshold, but this results in a larger false alarm rate. In contrast, the FF-RT performs better than the FT-RT for small ionospheric biases. However, the detection performance of FF-RT decreases as the ionospheric biases increase (e.g., when $\sigma_\iota = 4$ cm and $\sigma_\iota = 6$ cm). This is because the FF-RT becomes over-conservative owing to the weaker observation model from a larger unaccounted observation error. Among all these methods, the IM-RT performs best when there are large ionospheric errors. This implies that the IM-RT produces a more reliable ambiguity validation performance. Note that the false alarm and missed detection performance of IM-RT are not adequate as anticipated in the case of larger ionospheric biases. This is partially because of the integrity loss from the over-bounding of the non-perfect Fisher distribution. Moreover, the correctly fixed rate performance of FT-RT(1.5) and IM-RT is similar when $\sigma_\iota = 6$ cm. Nevertheless, there are more Type II errors when using the FT-RT(1.5) than the IM-RT, which implies that a loose detection threshold for the FT-RT is not suitable when the observation model is weak. The numerical comparisons with the popular ambiguity validation methods under different simulations demonstrate the best ambiguity validation performance for IM-RT.

Real-world test results and analysis

The GPS/BDS kinematic test was carried out in the urban area of Beijing. The base receiver is installed on the roof of the administration building located at the Academy of Opto-electronics, Chinese Academy of Sciences. The rover receiver was fixed on a car. The cutoff elevation is set to 10°. The trajectory of the rover receiver is shown in Fig. 6. The maximum baseline distance during the experiment is 13.8 km. To evaluate the kinematic test results, the positioning result in the ambiguity-fixed mode is used as a reference, which is produced by the commercial post-processing software (NovAtel GrafNav), and has a claimed accuracy of 5 cm (1σ). We collected and processed 6925 epochs of GPS and BDS dual-frequency data with a 1-s sampling period.

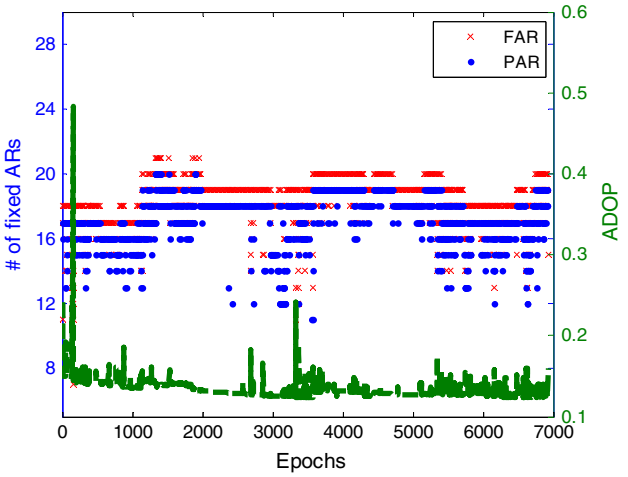

Fig. 7 ADOP values and the number of fixed ambiguities for FAR and PAR

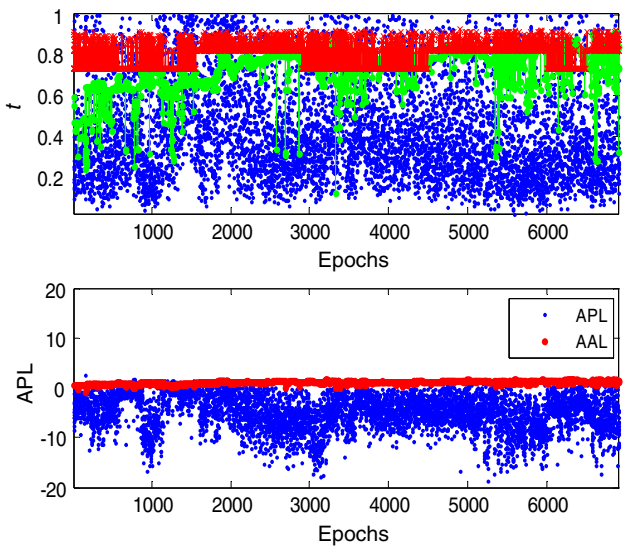

Fig. 8 Ratio values and thresholds for PAR + FF-RT and PAR + IM-RT. In the *top panel*, the *blue dot* indicates the ratio value, and the *green dot line* and the *red star line* indicate the threshold from FF-RT and IM-RT, respectively

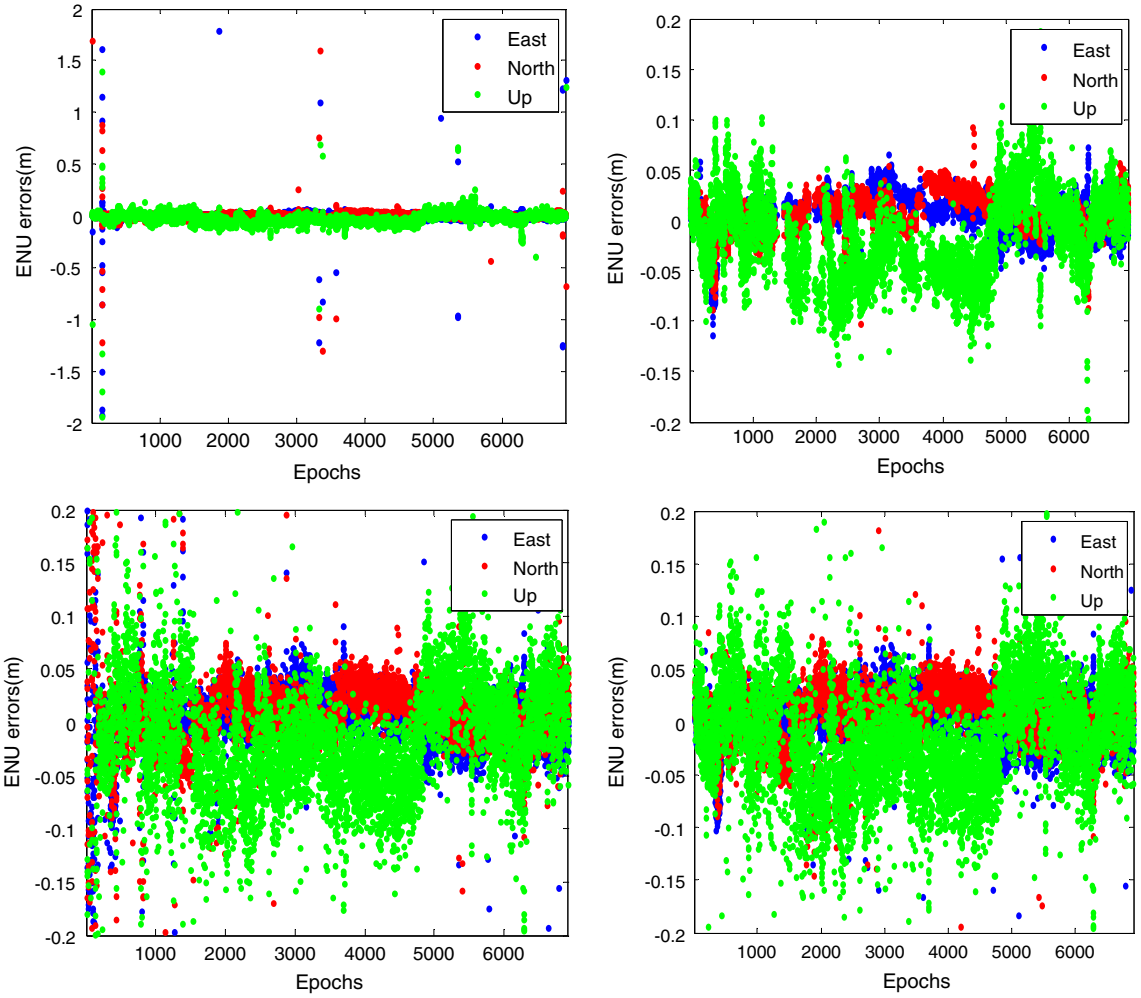

Fig. 9 Positioning errors using different methods. *Top left* FAR, *top right* FAR + FT-RT (3), *bottom left* PAR + FF-RT, *bottom right* PAR + IM-RT

Table 2 Positioning accuracy evaluation for different methods

	Fixed + float mode (cm)				Fixed mode (cm)				Continuity (%)
	STD			SEP (95 %)	STD			SEP (95 %)	
	E	N	U		E	N	U		
FAR	10.2	15.0	22.6	74	10.2	15.0	22.6	74	100
FAR + FT-RT(3)	15.4	15.9	31.4	52	5.8	1.8	4.3	27	79.6
PAR + FF-RT	14.0	15.9	27.8	49	8.4	8.1	13.3	44	86
PAR + IM-RT	13.2	14.5	20.1	41	8.5	7.0	10.9	35	91.2

The prior standard deviation settings for the code and phase observations are 30 cm and 0.3 mm, respectively. The geometry-based model is used in this kinematic experiment, and the positioning solutions are output instantaneously. Four methods to be examined include: the FAR without ambiguity validation, the FAR with FT-RT(3), the PAR + FF-RT, and the PAR + IM-RT. The fixed failure rate for the FF-RT is 10^{-3}. $N_{\min}$ for dual systems is 7, and otherwise, we only accept the float solution. The probabilities of false alarm and missed detection for the IM-RT are 10^{-3} and 5×10^{-3}, respectively, η is 0.05, and the search step length for α is 0.01. Note that the FAR without ambiguity validation solves the full ambiguity vector using the LAMBDA algorithm and simply takes the best ambiguity candidate as the ambiguity solution.

The ADOP value and the number of fixed ambiguities for PAR and FAR are shown in Fig. 7. The figure shows that a sufficiently small ADOP allows for a full AR. In contrast, a larger ADOP yields less fixed ambiguities because of the difficulty in satisfying the MSSR. In an extreme case, a large ADOP may result in less than $N_{\min}$ fixed ambiguities.

Figure 8 shows the detection results from the FF-RT and the proposed IM-RT. Figures 7 and 8 show that the detection threshold of FF-RT is sensitive to the ADOP value, which means that the FF-RT mainly relies on the model strength when given an expected failure rate and the number of ambiguities to be fixed. If the observation model is inconsistent with the data, the detection power of FF-RT decreases.

Figure 9 shows the positioning error of four AR methods in the ambiguity-fixed mode. The statistics of the position errors for the different methods in the fixed mode and fixed + float mode are listed in Table 2. Here, the continuity is defined as the ratio between the epochs of fixed mode and the epochs of fixed + float mode. By comparing the positioning accuracy of FAR and FAR + FT-RT, the necessity of ambiguity validation can be demonstrated, because the positioning accuracy in the fixed mode is significantly improved by FT-RT. The positioning accuracy of PAR + FF-RT in the fixed mode is barely satisfactory, which may be because there are many missed detection cases, as indicated by the large positioning errors. In contrast, the figure shows that the IM-RT produces more stable positioning errors, which can also be demonstrated by the numerical comparison between different ambiguity validation methods in the table. The large positioning errors of FAR, PAR + FF-RT, and PAR + IM-RT in the fixed mode are observed because of accepting the incorrectly fixed ambiguities; however, the spherical error probable (SEP 95 %) performance of IM-RT still achieves a 39-cm improvement over the FAR and a 9-cm improvement over the PAR + FF-RT. This demonstrates the superior ability of IM-RT in controlling Type II errors. The FAR + FT-RT(3) is more reliable than the IM-RT, which is reflected by the best positioning result in the fixed mode. Unfortunately, the FAR + FT-RT(3) has the worst continuity performance, because there are many false alarm cases that result from the over-conservative detection threshold. In contrast, the continuity of IM-RT is 11.6 and 5.2 % larger than the FAR + FT-RT and the PAR + FF-RT, respectively. This shows that the proposed IM-RT effectively controls Type I errors. Compared with the other three ambiguity validation methods, the IM-RT produces the best ambiguity validation results, because it simultaneously controls Type I and Type II errors.

Concluding remarks

Ambiguity validation is an important quality control procedure when applying high-precision GNSS positioning in safety–critical services. Unlike the traditional ratio tests that are carried out under the bias-free hypothesis and aim to verify whether or not the best ambiguity candidate is more likely than the second-best candidate, an integrity monitoring-based ratio test, named IM-RT, that monitors the effect of biases on the ambiguity validation, has been developed and tested. When compared with the popular ambiguity validation methods such as the FT-RT and the FF-RT, our simulation results have shown that the IM-RT provides a better ambiguity validation performance, which is reflected by the optimal balance performance between the false alarm and missed detection errors. The positioning accuracy and continuity results from the kinematic real-world experiment have also indicated that the IM-RT produces the best ambiguity validation performance. By deriving the detection threshold T from the false alarm rate requirement and the APL from the missed detection rate requirement, the IM-RT achieves the superior ambiguity validation performance using two innovations: (1) The IM-RT simultaneously controls the false alarm and missed detection errors, unlike the fixed detection threshold or single failure rate requirement used by traditional ratio tests, (2) to characterize the reliability of the AR, the IM-RT has two levels of protection because it sequentially applies the ratio test and the comparison of the constructed APL and AAL.

Although some parameters should be carefully chosen, e.g., the false alarm and missed detection probabilities and which is still an open problem, the IM-RT is an option for SoL navigational services. Furthermore, because the IM-RT belongs to the class of integer aperture estimators, the proposed algorithm can be extended to other high-precision positioning methods that require ambiguity validation such as PPP. Note that these results are based on limited data, and we are conducting further work to fully characterize the performance of the developed IM-RT under different operational conditions.

Acknowledgments The authors appreciate two anonymous reviewers for their editorial feedback and valuable suggestions. The authors are also very grateful to Dr. Sandra Verhagen from Delft University of Technology for the proofreading. This research was jointly funded by China Natural Science Foundation (Nos. 61304235, 41304034, 61273081), the Fundamental Research Funds for Central Universities (No. HEUCFD1431), the Key Laboratory for Urban Geomatics of National Administration of Surveying, Mapping, and Geoinformation (No. 20141205WY), and the Scientific Cooperation between China and the Netherlands programme '*Compass, Galileo and GPS for improved ionosphere modeling.*'

References

DeGroot MH, Schervish MJ (2011) Probability and statistics, 4th edn. Addison-Wesley, New York

Euler H, Schaffrin B (1991) On a measure for the discernibility between different ambiguity solutions in the static-kinematic GPS-mode. In: IAG symposia no. 107, kinematic systems in geodesy, surveying, and remote sensing. Springer, New York, pp 285–295

Feng S, Ochieng W, Samson J et al (2012) Integrity monitoring for carrier phase ambiguities. J Navig 64(1):41–58

Ge M, Gendt G, Rothacter M, Shi C, Liu J (2008) Resolution of GPS carrier-phase ambiguities in precise point positioning (PPP) with daily observations. J Geod 82(7):389–399

Han S (1997) Quality-control issues relating to instantaneous ambiguity resolution for real-time GPS kinematic positioning. J Geod 71:351–361

Hwang P, Brown RG (2006) RAIM-FDE revisited: a new breakthrough in availability performance with NIORAIM (Novel Integrity Optimized RAIM). J Inst Navig 53(1):41–52

Khanafseh S, Pervan B (2010) A new approach for calculating position domain integrity risk for cycle resolution in carrier phase navigation systems. IEEE Trans Aero Electron Syst 46(1):296–307

Lee J, Pullen S, Enge P (2009) Sigma overbounding using a position domain method for the local area augmentation of GPS. IEEE Trans Aero Electron Syst 45(4):1262–1274

Leick A, Rapoport L, Tatarnikov D (2015) GPS satellite surveying, 4th edn. Wiley, New York

Li T, Wang J (2014) Analysis of the upper bounds for the integer ambiguity validation statistics. GPS Solut 18(1):85–94

Li Z, Yuan Y, Li H, Huo X (2012) Two-step method for the determination of the differential code biases of Compass satellites. J Geod 86(11):1059–1076

Li B, Verhagen S, Teunissen PJG (2014) Robustness of GNSS integer ambiguity resolution in the presence of atmospheric biases. GPS Solut 18(2):283–296

Parkins A (2011) Increasing GNSS RTK availability with a new single-epoch batch partial ambiguity resolution algorithm. GPS Solut 15(4):391–402

Teunissen PJG, Kleusberg A (1998) GPS for geodesy, 2nd edn. Springer, Berlin

Teunissen PJG, Verhagen S (2009) The GNSS ambiguity ratio-test revisited: a better way of using it. Surv Rev 41(312):138–151

Teunissen PJG, Joosten P, Tuberius CCJM (1999) Geometry-free ambiguity success rates in case of partial fixing. In: Proceedings of ION NTM-99, Institute of Navigation, San Diego, CA, January 25–25, pp 201–207

Tiberius C, Jonge P (1995) Fast positioning using the LAMBDA method. In: Proceedings of DSNS-95, Bergen, Norway, Bergen, Norway, Paper 30, p 8

Verhagen S, Teunissen PJG (2013) The ratio-test for future GNSS ambiguity resolution. GPS Solut 17(4):535–548

Verhagen S, Odijk D, Teunissen PJG, Huisman T (2010) Performance improvement with low-cost multi-GNSS receivers. In: Proceedings of 5th ESA workshop on satellite navigation technologies and European workshop on GNSS signals and signal processing (NAVITEC), pp 1–8

Wang J, Stewart MP, Tsakiri M (1998) A discrimination test procedure for ambiguity resolution on the fly. J Geod 72(11):644–653

Liang Li joined Harbin Engineering University as a lecturer in 2013. This paper was finished at Academy of Opto-electronics (AOE), Chinese Academy of Sciences (CAS), where he was working as a research associate for 2 years. His research interests include: GNSS navigation and integrity monitoring.

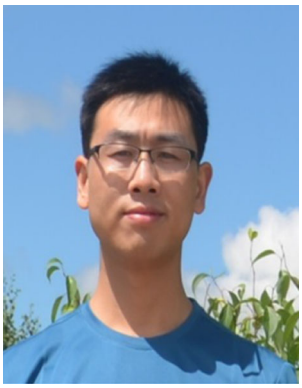

Zishen Li is currently a research assistant at AOE, CAS. He received the Ph.D. degree in Geodesy and Surveying Engineering from the Institute of Geodesy and Geophysics, in 2013. His current research activities are related to the ionospheric time delay correction for GNSS/BDS users.

Hong Yuan is currently a professor and the director of Navigation Department, AOE, CAS. He received the Ph.D. degree in Shanxi Astronomy Observatory, CAS, in 1995 and the B.Sc. degree in Xidian University, in 1991. His interest currently focuses on the ionospheric modeling and multi-sensors-based navigation.

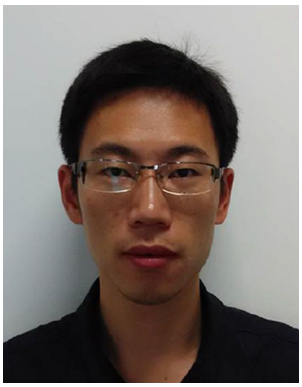

Liang Wang is currently a research student at AOE, CAS, and University of Chinese Academy of Sciences. His current research activities are related to the high-precision real-time BDS/GNSS positioning.

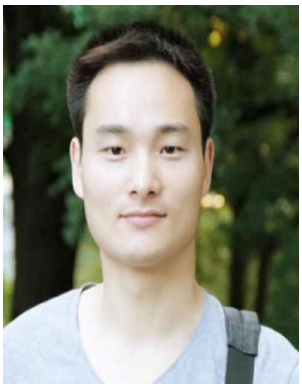

Yanqing Hou is a Ph.D. candidate in Geoscience and Remote Sensing Department in Delft University of Technology in the Netherlands. His research interests include partial ambiguity resolution under multi-GNSS constellation, bias-affected ambiguity resolution, and integrity monitoring.